Fusion by diffusion. II. Synthesis of transfermium elements in cold fusion reactions

W. J. Świątecki,[1] K. Siwek-Wilczyńska,[2] and J. Wilczyński[3]
[1]*Nuclear Science Division, Lawrence Berkeley National Laboratory, Berkeley, California 94720, USA*
[2]*Institute of Experimental Physics, Warsaw University, Hoża 69, 00-681 Warsaw, Poland*
[3]*Andrzej Sołtan Institute for Nuclear Studies, 05-400 Otwock-Świerk, Poland*
(Received 3 August 2004; published 7 January 2005)

We describe a method of estimating cross sections for the synthesis of very heavy nuclei by the fusion of two lighter ones. The cross section is considered to be the product of three factors: the cross section for the projectile to overcome the Coulomb barrier, the probability that the resulting composite nucleus reaches the compound nucleus configuration by a shape fluctuation treated as a diffusion of probability in one dimension, and the probability that the excited compound nucleus survives fission. Semi-empirical formulas for the mean Coulomb barrier height and its distribution around the mean are constructed. After overcoming the Coulomb barrier the system is assumed to be injected into an "asymmetric fission valley" by a rapid growth of the neck between the target and projectile at approximately frozen asymmetry and elongation. Diffusion in the elongation coordinate in this valley can occasionally bring the system over the saddle separating the injection point from the compound nucleus configuration. This is the stage that accounts for the hindrance to fusion observed for very heavy reacting systems. The competition between deexcitation of the compound nucleus by neutron emission and fission is treated by standard methods, but an interesting insight allows one to predict in an elementary way the location of the maximum in the resulting excitation function. Adjusting one parameter in the theory causes the calculated peak cross sections to agree within about a factor of 2 or so with 12 measured or estimated values for "cold" one-neutron-out reactions where targets of ^{208}Pb and ^{209}Bi are bombarded with projectiles ranging from ^{48}Ca to ^{70}Zn. The centroids of the excitation functions agree with theory to within 1 or 2 MeV for the six cases where they have been determined, and their widths are reproduced. "Hot" fusion reactions, where several neutrons are emitted, are not treated, except that a comparison is made between the hindrance factors in cold and hot reactions to make elements with atomic numbers 112 to 118. The calculated diffusive hindrances in the hot reactions are less unfavorable by 4 to 5 orders of magnitude.

DOI: 10.1103/PhysRevC.71.014602 PACS number(s): 25.70.Jj, 25.70.Gh

I. INTRODUCTION

This paper continues the study of fusion excitation functions along the lines of our early work [1], which will be referred to as Part I. (The present paper goes beyond [1] in several respects. Reactions with ^{209}Bi targets have been included, the calculations of the Coulomb barrier heights and the diffusion stage have been much improved, and the diffusion hindrance factors in hot reactions have been calculated. Reference [2] should also be consulted for background information and relevant results.) The excitation functions in question refer to nuclear reactions where a very heavy nucleus is synthesized by the fusion of two lighter ones. Our theory approximates the cross section for such reactions by the product of three factors, written schematically as

$$\text{Fusion} = \text{Stick} \times \text{Diffuse} \times \text{Survive}. \quad (1)$$

Here "Stick" stands for the cross section needed for the target and projectile to form a composite system (essentially the cross section for overcoming the Coulomb barrier). "Diffuse" stands for the probability that the composite system reaches the compound-nucleus configuration in the presence of thermal shape fluctuations, treated as a diffusion of probability. "Survive" represents the probability that the compound nucleus survives fission.

In [1,2] as well as in the present paper we focus attention (except for Sec. VI) on reactions where the target is either ^{208}Pb or ^{209}Bi, and the projectiles range from ^{48}Ca to ^{86}Kr designed, after fusion, to form compound nuclei with atomic numbers $Z = 102, 103, \ldots, 119$ (Fig. 1). In such "cold" reactions the bombarding energy can be chosen sufficiently low so that the compound nucleus (if formed) can deexcite by the emission of a single neutron (followed by γ rays). In a future publication we hope to apply our theory to "hot" reactions, where more than one neutron is emitted (Fig. 1).

At the present time, there exists information on 12 one-neutron-out excitation functions resulting in the production of elements with $Z = 102, 103, \ldots, 112$ [3–6]. The measured (or estimated) peak cross sections are shown, respectively, as solid or open circles in Fig. 2; they constitute the data set that will be used to test our proposed scheme based on Eq. (1). In what follows, Secs. II–IV specify the expressions used in the calculation of the three factors in Eq. (1), as illustrated by the three lines in Fig. 2. The calculated excitation functions are confronted with measurements in Sec. V. Section VI compares for cold and hot reactions the hindrances to fusion associated with the diffusion stage. The results are further discussed and summarized in Sec. VII.

II. STICKING

The classical formula for the cross section to overcome a barrier B encountered at separation R between two mass

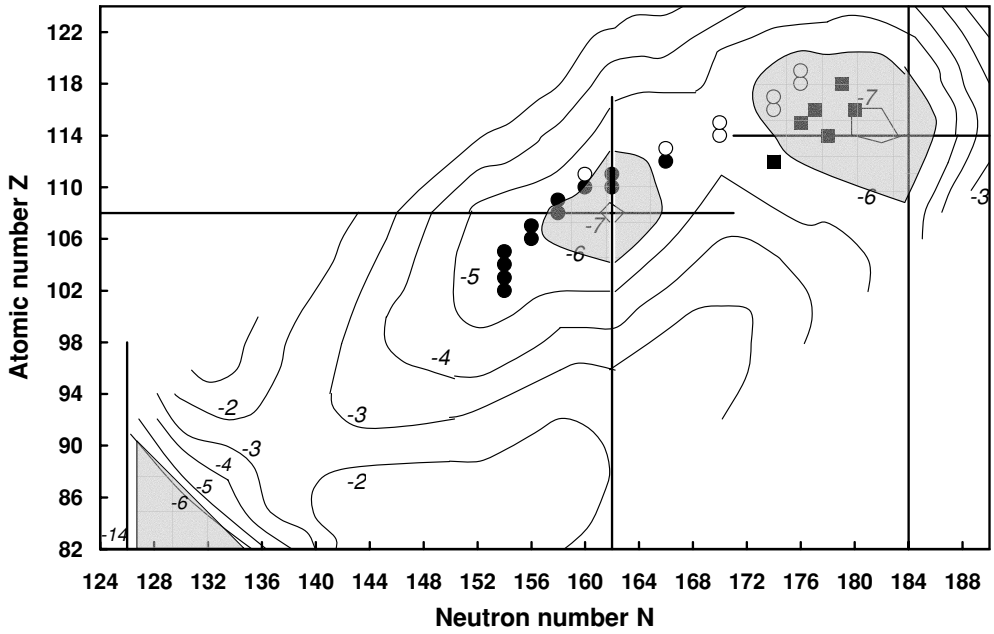

FIG. 1. Contours of calculated shell corrections in MeV for very heavy nuclei [26]. The circles show the locations of the compound nuclei (landing places) in one-neutron-out cold fusion reactions with ^{208}Pb and ^{209}Bi targets bombarded by the following projectiles: ^{48}Ca, ^{50}Ti, ^{54}Cr, ^{58}Fe, ^{62}Ni, ^{64}Ni, ^{70}Zn, ^{76}Ge, ^{82}Se, and ^{86}Kr. The solid circles refer to reactions where synthesis has been achieved. The squares refer to landing places in hot fusion reactions in which ^{48}Ca projectiles bombarded targets of ^{238}U, ^{244}Pu, ^{243}Am, ^{245}Cm, ^{248}Cm, and ^{249}Cf, and several neutrons were emitted.

points colliding with center of mass energy E reads

$$\begin{aligned} \sigma(\text{stick}) &= \pi R^2 \left(1 - \frac{B}{E}\right) \qquad \text{for } E \geqslant B, \\ \sigma(\text{stick}) &= 0 \qquad\qquad\qquad\quad \text{for } E \leqslant B. \end{aligned} \tag{2}$$

Multiplying $\sigma(\text{stick})$ by E and dividing by πR^2 we find for the energy-weighted reduced cross section $y \equiv \sigma E/\pi R^2$, the expression

$$\begin{aligned} y &= E - B \qquad \text{for } E \geqslant B, \\ y &= 0 \qquad\quad \text{for } E \leqslant B. \end{aligned} \tag{3}$$

This expression, consisting of segments of two straight lines with a slope discontinuity at $E = B$, may be readily generalized into a smoothed expression that reproduces much more closely the smooth measured energy-weighted reduced

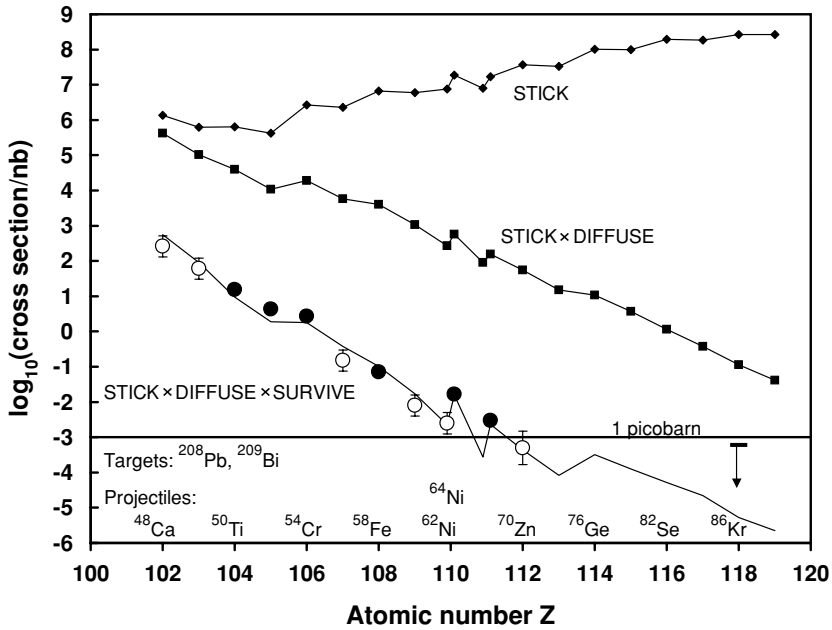

FIG. 2. The lowest line shows logarithms of calculated peak cross sections for the synthesis of elements with atomic numbers $Z = 102$ to $Z = 119$, in one-neutron-out reactions using targets of ^{208}Pb and ^{209}Bi bombarded with the projectiles listed along the Z axis. (The calculated values were multiplied by 0.7 to allow approximately for the dispersion of the beam energy in a typical target foil.) The solid circles refer to measured values, the open circles to estimates (more likely to be under than overestimates because the maxima in the excitation functions had not been located). The uppermost curve shows the calculated cross sections for overcoming the Coulomb barrier; the middle curve, the cross sections for forming a compound nucleus.

cross sections. This is done as follows. Differentiating Eq. (4) with respect to E results in a step function, and a second differentiation produces a delta function at $E = B$. Now replace the delta function by a normalized Gaussian of range v, viz. $(v\sqrt{\pi})^{-1}\exp(-X^2)$, where $X = (E - B)/v$, and reverse the differentiations. The first integration gives the smoothed step function $(1 + \text{erf}\, X)/2$, and the second gives a smoothed energy-weighted reduced cross section, from which follows the generalized expression for $\sigma(\text{stick})$:

$$\sigma(\text{stick}) = \pi R^2 \frac{v}{2E}\left[X(1 + \text{erf}\, X) + \frac{1}{\sqrt{\pi}}\exp(-X^2)\right]. \tag{4}$$

In the language of the "barrier distribution" scheme of Rowley, Satchler, and Stelson [7], we have introduced a Gaussian distribution of barriers [8]. However, our empirical Gaussian smoothing may be simulating, at least approximately, any kind of smoothing (for example, that due to quantal barrier penetration) in addition to that due to actual distributions of barriers associated with nuclear deformations and vibrations.

Eq. (4) was fitted to accurately measured fusion cross sections for a nucleus $(A_1 Z_1)$ colliding with a nucleus $(A_2 Z_2)$ at energies around the barrier for 45 reactions ranging from ^{40}Ca + ^{40}Ca to ^{40}Ca + ^{194}Pt. (See [8] for an updated version of such fits.) This resulted in 45 sets of fitted values of R, B, and v. Note that in a logarithmic plot of σ given by Eq. (4), different values of R result in a mere vertical shift of the curve, the *intrinsic* shape of $\log\sigma$ being determined by B and v alone. Hence the optimum fits to the data (which, for any given reaction, turned out to be extremely accurate [8]) yield 45 pairs of values of B and v, which do not depend on R. These values are plotted in Figs. 3–5 as functions of the conventional Coulomb parameter $z \equiv Z_1 Z_2/(A_1^{1/3} + A_2^{1/3})$, up to about $z = 170$. The question now arises of extrapolating these empirical trends to the reactions of interest, with z values ranging from about 170 to 300. In the case of the barriers, we made the extrapolation by first supplementing the empirical points in Fig. 3 by barriers calculated using the parameterless Proximity theory of [9]. (Only a sampling of the Proximity barriers is displayed.) A parabolic fit to the Proximity barriers passing through the origin in Fig. 3 indicates an overestimate by several MeV of the 45 measured barriers, indicating the need to adjust the Proximity barriers to the data. (See also [8].) Figure 4 shows the result of lowering the Proximity barriers by 3 MeV. The following cubic in z now provides a reasonable representation of all the points:

$$B = 0.85247z + 0.001361z^2 - 0.00000223z^3\ \text{MeV}. \tag{5}$$

We adopted this cubic as our extrapolation formula for the mean barrier energy. (Another extrapolation scheme is suggested in [8].)

The extrapolation of the trend of v in Fig. 5 is more difficult. To allow for some, at least, of the anticipated structural features in the colliding nuclei, we experimented with several semi-empirical formulas for v, of which we adopted the following:

$$v = CB\sqrt{W_1^2 + W_2^2 + W_0^2}. \tag{6}$$

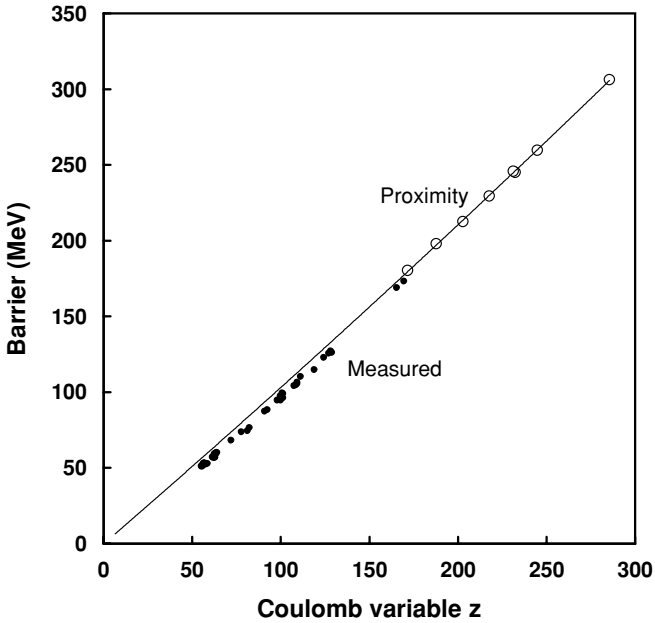

FIG. 3. The black dots are Coulomb barriers for 45 reactions deduced from accurately measured excitation functions fitted by Eq. (4) in the text. The circles are theoretical "Proximity" barriers [9] calculated for eight reactions ranging from ^{48}Ca to ^{86}Kr on ^{208}Pb. The plots are against the Coulomb parameter $z = Z_1 Z_2/(A_1^{1/3} + A_2^{1/3})$. The curve, a parabolic fit to the circles, shows that the Proximity theory overestimates measurements by several MeV.

Here B is the barrier given by Eq. (5) and C is an adjustable parameter. W_1 and W_2 are the rms distributions of the radius vectors specifying the surfaces of the projectile and target, whose mean radii are R_1 and R_2 and whose quadrupole

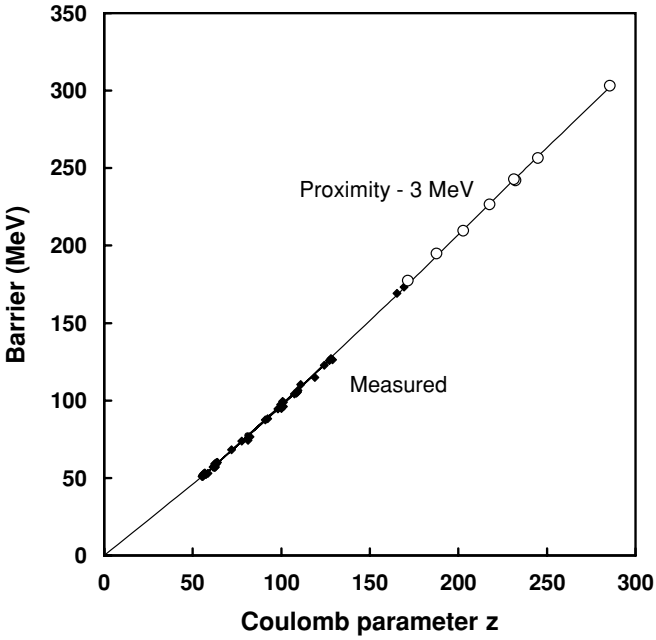

FIG. 4. This is like Fig. 3, but the Proximity points have been moved down by 3 MeV. The curve is a cubic fit to all the points.

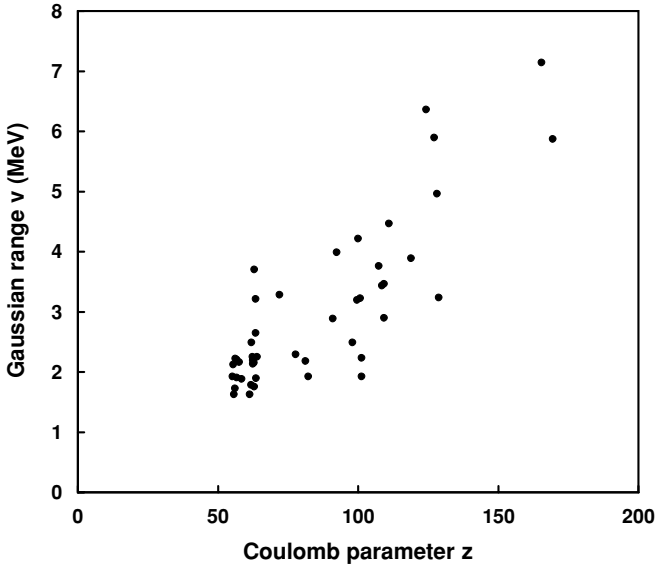

FIG. 5. The Gaussian range parameters v, deduced from fits of Eq. (4) to the excitation functions for 45 reactions, are plotted against the Coulomb parameter z.

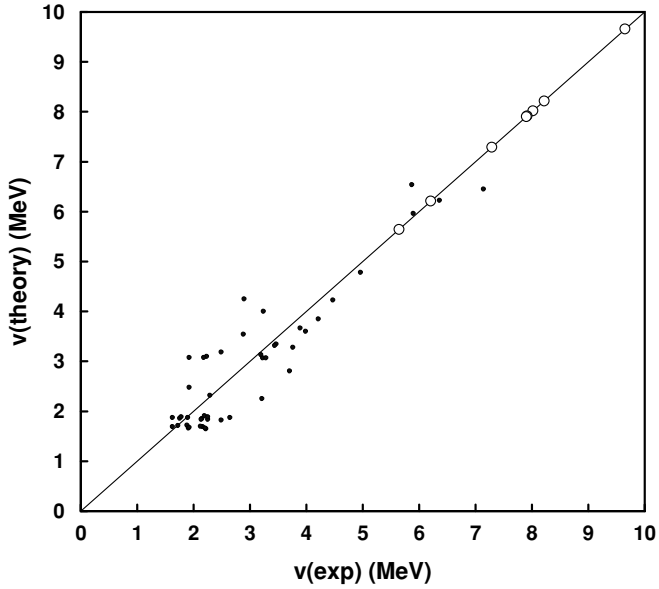

FIG. 6. The theoretical ranges v given by Eq. (6) are plotted against measured values. The line along the diagonal indicates the extrapolation of the theory to the heavier reactions shown by circles, ranging from ^{48}Ca to ^{86}Kr on ^{208}Pb.

deformation parameters are β_1 and β_2. It is readily shown that

$$W_i^2 = \frac{R_i^2 \beta_i^2}{4\pi}. \tag{7}$$

We took $R_i = 1.14 A_i^{1/3}$ fm and β_i as given under the heading "β_2" in [10]. (We disregarded multipolarities higher than the quadrupole.) The quantity W_0 in Eq. (6) is a second adjustable parameter designed to represent, at least roughly, nuclear vibrations, quantal barrier penetrability, etc.

Fitting Eq. (6) to the collection of measured v values, we found $C = 0.07767$ fm^{-1} and $W_0 = 0.41$ fm. The (limited) success of this procedure is illustrated in Fig. 6, where the parameterized values of v are plotted against the empirical ones. The straight line along the diagonal indicates the result of extrapolation to the reactions of interest up to $^{86}\mathrm{Kr} + {}^{208}\mathrm{Pb}$. The rms deviation of the theoretical from the experimental values of the Gaussian range v is 0.570 MeV. There is much room for improvement here. We note, however, that for the heaviest reactions, beyond about $Z = 112$, sticking becomes an over-the-barrier process, and the sticking cross section tends to the geometric limit, independent of v.

III. DIFFUSION

For relatively light colliding nuclei, overcoming the Coulomb barrier leads automatically to the formation of the compound nucleus. The cross section for the synthesis is then the product of the cross section to overcome the Coulomb barrier and the probability to survive fission:

$$\text{Fusion} = \text{Stick} \times \text{Survive}. \tag{8}$$

It has long been known that for heavier systems the observed production cross sections begin to show exponentially increasing deviations from such a product. A qualitative understanding of this hindrance to fusion in heavy systems has been available since the 1980s and has to do with a simple geometrical feature. Figure 7 shows how, for relatively light colliding systems, the overall length of the target and

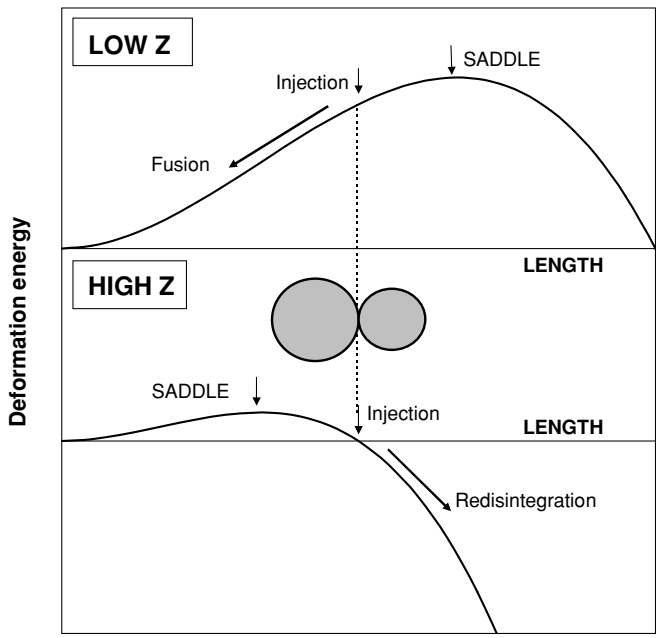

FIG. 7. The qualitative explanation of the appearance of a hindrance to fusion for very heavy reactions. For light reacting systems, the tangent configuration is on the inside of the saddle-point shape in elongation space. Beyond a critical size of the reacting system the saddle moves inside the tangent configuration and an uphill diffusion is necessary for the system to reach the compound nucleus configuration.

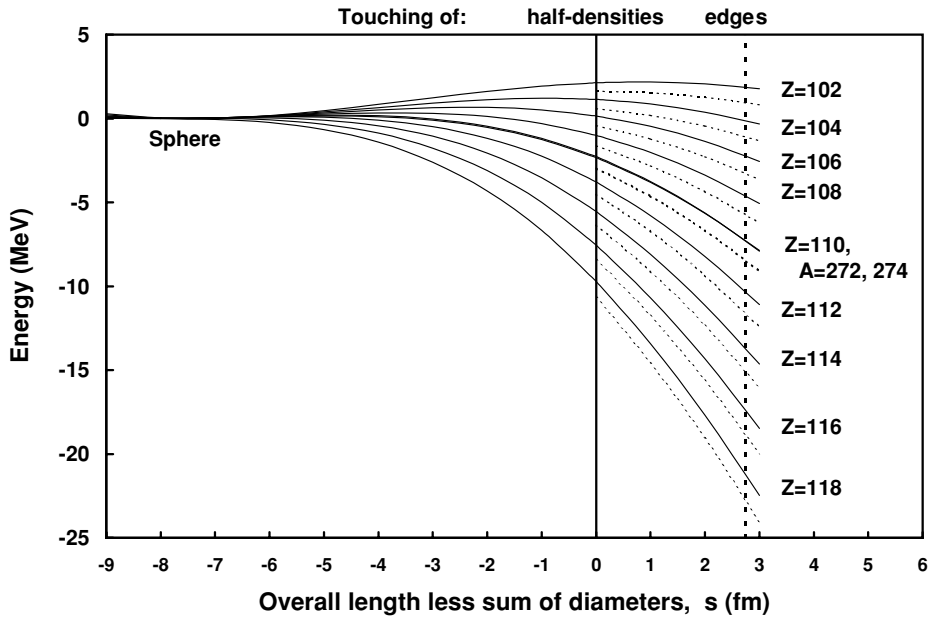

FIG. 8. The macroscopic deformation energies along the asymmetric fission valley for 20 reactions ranging from ^{48}Ca + ^{208}Pb to ^{86}Kr + ^{209}Bi, as functions of s, equal to the excess of the length of the configuration over the sum of the target and projectile diameters. In the entrance channel of two approaching nuclei, a length specified by $s = 0$ would correspond to contact of the half-density contours, and $s \approx 2.74$ fm to the contact between the classical turning points of the fastest nucleons in the two nuclei (the nucleons at the Fermi energy).

projectile configuration at contact is less than the length of the saddle-point configuration guarding the compound nucleus against disintegration. Hence, after contact and neck growth, the composite system is likely to find itself on the *inside* of the saddle-point barrier, and fusion follows automatically. But for progressively heavier systems, the saddle-point shape begins to shrink rapidly when the fissility parameter x, the ratio of the electrostatic to twice the surface energy of the spherical configuration, exceeds about 0.7. (The macroscopic saddle shape tends to the sphere as x tends to one. For asymmetric systems, an effective fissility $x_{\rm eff}$ replaces x [11].) As a result, beyond a critical size of the target-projectile combination, the composite nucleus will find itself *outside* the saddle-point barrier, and automatic fusion will not take place. In fact, in a classical dynamic calculation without fluctuations, the system would redisintegrate without ever having reached the compound nucleus configuration. An infinite hindrance to fusion would have set in [11].

Looking apart from quantal effects, only thermal shape fluctuations can cause a system "on the wrong side of the barrier" to nevertheless diffuse up hill and, with some probability P(diffuse), to reach the compound nucleus configuration. The simplest model that illustrates the essence of such a diffusion process is the one-dimensional Brownian motion of a particle suspended in a viscous fluid at temperature T in the presence of a repulsive parabolic potential $V(L) = -b(L - L_{\rm max})^2/2$, where $L_{\rm max}$ locates the maximum in $V(L)$. In our case, the position L of the Brownian particle translates into the fluctuating length of the fusing system. The equation describing the probability $W(L, t)$ to find the system with coordinate L at time t is the Smoluchowski partial differential equation [12]

$$G\frac{\partial W}{\partial t} = -(bLW)' + TW''. \tag{9}$$

Here G is proportional to the viscosity of the fluid in the case of the Brownian particle, or to the dissipation acting in the length degree of freedom L in the case of fusion. Primes denote partial differentiations with respect to L.

As discussed in Part I, the solution for $W(L, t)$ corresponding to starting at $t = 0$ with a delta function distribution at some initial elongation (the "injection point" $L_{\rm inj}$) is a monotonically swelling Gaussian distribution in L, sliding away from the maximum in $V(L)$. (See [1] for the explicit expression for this Gaussian.) As t tends to infinity, the portion of the Gaussian distribution that managed to overcome the barrier tends to the following expression (independent of G):

$$P(\text{diffuse}) = \tfrac{1}{2}(1 - \text{erf}\sqrt{H/T}) = \tfrac{1}{2}\,\text{erfc}\sqrt{H/T} \quad \text{if } L_{\rm inj} \geqslant L_{\rm max}, \tag{10}$$

$$P(\text{diffuse}) = \tfrac{1}{2}(1 + \text{erf}\sqrt{H/T}) \quad \text{if } L_{\rm inj} \leqslant L_{\rm max}. \tag{11}$$

Here H is the height of the barrier opposing fusion along the asymmetric fission valley, as seen from the injection point. T is the temperature (of the fluid or of the fusing system), assumed constant. In this bare-bones representation of the diffusion stage, the only quantity needed to estimate P(diffuse), i.e., the hindrance to fusion, is the ratio H/T.

As explained in [1] and [2], we estimate H/T by noting that at a point near contact between two approaching fluid spheres, a loss of equilibrium takes place against a rapid growth of a neck. The system is then injected from near contact into an "asymmetric fission valley." defined by minimizing the potential energy of the system at fixed asymmetry and elongation. Using the parameterization of the nuclear shapes by two spheres joined smoothly by a third quadratic surface of revolution [13], this minimization gives a definite energy along the bottom of the asymmetric fission valley in its dependence on the length L of the system. (For details see App. A.) The result is shown in Fig. 8. Here the (purely macroscopic) deformation energy is plotted for 20 compound nuclei with $Z = 102$–119. The abscissa is the overall length L of the system less the sum of the diameters of the original reacting partners. Thus $s = 0$ corresponds to a length equal

to the length of the tangent configuration, and $s = 3$ fm to a length in which the effective surfaces of the approaching nuclei are 3 fm apart. It is in this range of separations, of the order of the nuclear surface diffuseness, that one might expect the loss of equilibrium against neck formation to take place. The deformation energies in Fig. 8 were calculated by the above-mentioned minimization procedure down to $s = 0$, and continued by a smoothly joined cubic, constrained to be stationary at the spherical configuration, i.e., at a value of $L = L_0$ equal to the diameter of the compound nucleus. (See App. A for details.) For any assumed value of L (or s) at injection, one may then deduce the height of the barrier H that has to be overcome by diffusion. If one makes the assumption that on reaching the bottom of the asymmetric fission valley the dynamic evolution is strongly damped, so that the collective kinetic energy is negligible, the thermal excitation energy of the system follows from the difference between the total available energy and the potential energy at $L_{\rm inj}$. The temperature T may then be estimated in the usual way. At the present time, we are not in a position to calculate from first principles the precise value of s at which, in the case of diffuse surfaces, loss of equilibrium takes place against neck growth, or to deduce the (effective) value of L at which the diffusion process begins. We shall consider this value of L, as specified by s, to be an adjustable parameter of our theory. In fact, it will be the only adjustable parameter. On physical grounds the value of s ought to be somewhere between about zero and 3 fm.

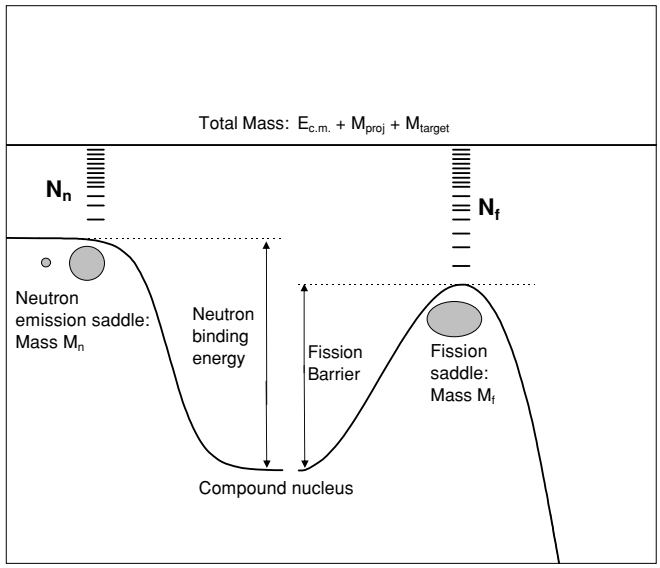

FIG. 9. The relative decay probability by neutron emission or fission is the ratio N_n/N_f of the number of levels ("channels") in the energy intervals between the total available energy (or mass in energy units) and the masses of the neutron emission or fission saddle points, M_n or M_f, respectively. The mass of the compound nucleus does not enter into this ratio. The middle part of the figure could be erased without any loss of relevant information, showing that neither the fission barrier height nor the neutron separation energy, nor any other property of the compound nucleus is required for the calculation of the relative decay probability.

IV. SURVIVAL

In the case when an excited system can decay by overcoming two distinct saddle-point passes in configuration space (in our case by fission and neutron emission), the canonical transition state theory of reaction rates gives for the relative decay probability (i.e., the ratio of the partial decay widths Γ_n/Γ_f) the elementary relation

$$\Gamma_n/\Gamma_f = N_n/N_f. \tag{12}$$

Here N_n and N_f are measures of the phase spaces available to the "activated complexes" or "transition states." (These are defined as the systems described by all the degrees of freedom of the saddle-point configurations except for the disintegration variables.) For a system in which the degrees of freedom are quantized, N_f is the number of levels (channels) in the activated complex in the energy slot between the energy V_f of the fission saddle configuration and the total available energy E (Fig. 9.) In the case of neutron emission, the formal saddle-point configuration is the residual nucleus of mass number $A - 1$ with a neutron (just) outside it. The quantity N_n is then the number of relevant levels of this configuration in the slot between its energy V_n and E. Treating the neutron-emission and fission processes in an identical way [14] we find

$$\frac{N_n}{N_f} = \frac{\int_0^{U_n} \rho_n(\epsilon)d\epsilon}{\int_0^{U_f} \rho_f(\epsilon)d\epsilon}. \tag{13}$$

Here $\rho_n(\epsilon)$ and $\rho_f(\epsilon)$ are the level densities characterizing the two saddle-point configurations (Fig. 9.) The calculation of N_n and N_f is essentially as described in Part I, but because of slight modifications, App. B lists the actual equations used in the present paper.

Note that the ratio N_n/N_f is independent of the properties of the compound nucleus, such as its ground state mass, its fission barrier, neutron separation energy, shell effect, and level density (Fig. 9.) The implication that Γ_n/Γ_f is independent of the fission barrier of the compound nucleus is valid so long as equating Γ_n/Γ_f to N_n/N_f is justified. Whether or not this result of the canonical transition state theory continues to be valid (at least approximately) even when the fission barrier is very small (and eventually vanishes) is not clear.

The probability that the compound nucleus evaporates just one neutron is the product of the probability to emit a neutron rather than fission in the first stage of the deexcitation process *times* the probability $P_<$ that, after the emission of the neutron, the excitation energy is less than the threshold $E_{\rm th}$ for second chance fission or second neutron emission (whichever is lower). Thus

$$P(\text{survive}) = \frac{\Gamma_n}{\Gamma_t} P_<, \tag{14}$$

where

$$\Gamma_t = \Gamma_n + \Gamma_f. \tag{15}$$

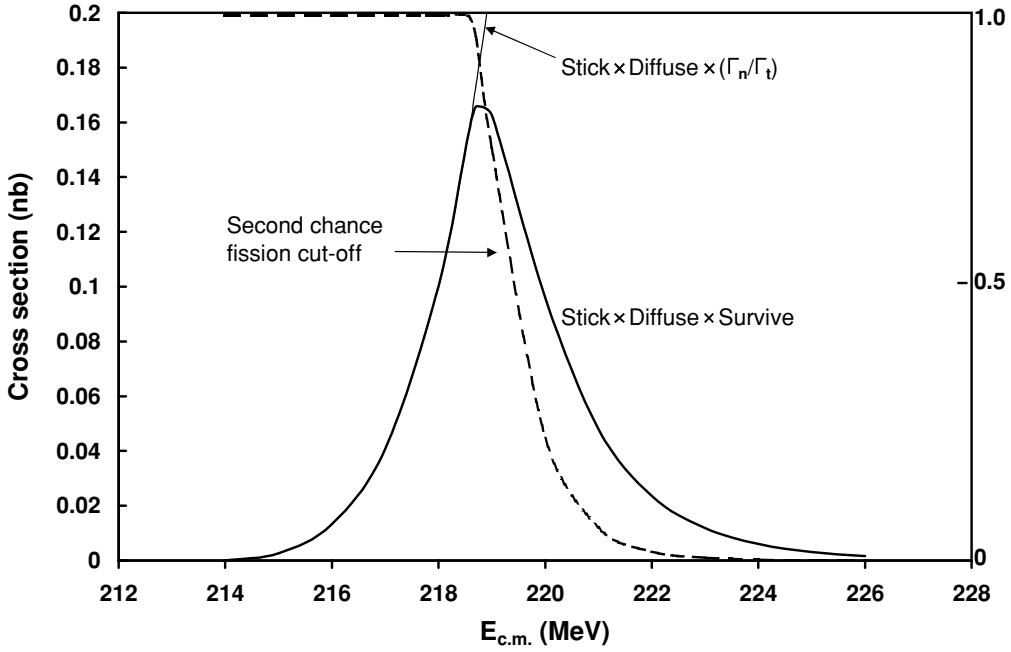

FIG. 10. The anatomy of a one-neutron-out excitation function for the reaction $^{58}\mathrm{Fe} + {}^{208}\mathrm{Pb} \rightarrow {}^{265}108 + n$ (see text).

In what follows we disregard γ emission, which becomes negligible compared to neutron emission or fission almost as soon as the latter have become energetically possible.

Using a standard neutron evaporation spectrum proportional to $k\exp(-k/T)$, where k is the neutron's kinetic energy and T the temperature of the transition state for neutron emission, $P_<$ follows by integrating the neutron spectrum from $E - E_{\mathrm{th}}$ to infinity, with the result

$$P_< = \left(1 + \frac{K}{T}\right)\exp\left(-\frac{K}{T}\right) \qquad \text{if } K \geqslant 0, \tag{16}$$

$$P_< = 1 \qquad \text{if } K \leqslant 0, \tag{17}$$

where $K = E - E_{\mathrm{th}}$.

V. THE EXCITATION FUNCTIONS

A. Comparison of theory and measurement

The three factors in Eq. (1), as calculated using the formulas described above, are all functions of the center of mass energy E, and their product gives a theoretical excitation function. It contains one adjustable quantity, the effective elongation L (as specified by the parameter s) at which the diffusion process in the asymmetric fission valley is assumed to begin. The calculated peak cross sections, corrected approximately for the dispersion of the beam energy in the target, are compared with measurements in Fig. 2. The value of s was adjusted to be 1.6 fm. Changing s pivots the calculated curve by changing its overall slope, with the point for $Z = 102$ approximately fixed. This is because for the $^{48}\mathrm{Ca} + {}^{208}\mathrm{Pb}$ reaction ($Z = 102$) there is essentially no hindrance to fusion, so that this cross section is very insensitive to changes of s (see Fig. 8). For larger Z the effect of changing s becomes progressively greater. Figure 2 also shows how the separate contributions to the calculated cross sections depend on Z.

Figure 10 illustrates the factors determining the appearance of the excitation function in the case of the reaction $^{58}\mathrm{Fe} + {}^{208}\mathrm{Pb} \rightarrow {}^{265}108 + n$. The reaction channel for neutron emission opens near the effective threshold $E_{\mathrm{c.m.}} = 213.8$ MeV, after which the cross section increases rapidly, since all three factors (stick, diffuse, and survive) increase with energy. (The word "effective" means that the actual energetic threshold has been augmented by a correction to allow for the even-odd effect in the level density; see App. B.) This exponential-like increase is terminated abruptly when the channel for fission after neutron emission ("second chance fission") opens near the effective threshold $E_{\mathrm{th}} = 218.9$ MeV. To avoid fission beyond this energy, the emitted neutron must carry off as kinetic energy the excess $E - E_{\mathrm{th}}$. As mentioned in the previous section, the probability that this happens decreases exponentially, with a characteristic fall-off range of the order of the temperature of the residual nucleus $A - 1$ (less than 1 MeV in the cases of interest). This decrease, indicated by the dashed curve in Fig. 10, is sufficiently abrupt to reverse the original exponential-like growth of the cross section. The resulting excitation function consists then of an exponential-like increase below E_{th} and an exponential-like decrease above E_{th}, with a maximum very close to the threshold for second chance fission. In the general case, E_{th} would be the threshold for second chance fission or for second neutron emission, whichever was lower. (In the cases of interest here, the former is lower.) This leads to the "optimum energy rule" from [1], which we restate in a more general form as

The optimum center-of-mass bombarding energy in a one-neutron-out heavy ion fusion reaction exceeds by a small amount (usually ∼0.3 MeV) either the effective mass of the fission saddle point of the residual nucleus ($A - 1$) plus the

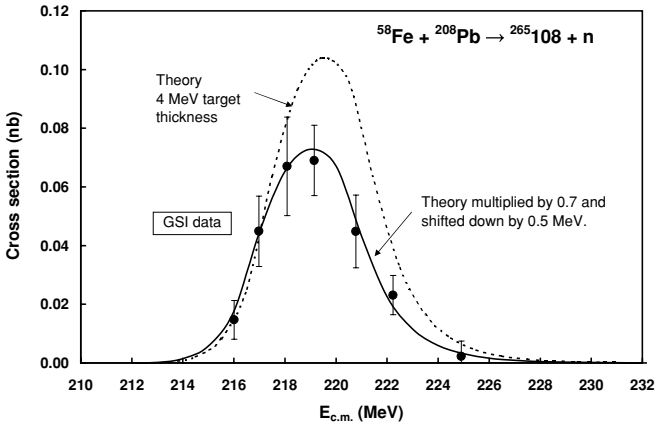

FIG. 11. Comparison of the theoretical excitation function for the ^{58}Fe + ^{208}Pb → ^{265}108 + n reaction with measurements. The dotted curve is the theoretical excitation function convoluted with a (rectangular) spread in the center of mass beam energy of 4 MeV caused by the finite target thickness. The solid curve results from multiplying the dotted curve by 0.7, and shifting it down by 0.5 MeV. These numbers are a measure of the discrepancy between theory and experiment. Note that the predicted width of the excitation function agrees with measurement.

mass of a neutron minus the masses of target and projectile, or the effective mass of the residual nucleus ($A - 2$) plus the mass of two neutrons minus the masses of target and projectile – if the latter quantity is lower.

(The word "effective" again refers to the correction applied to the saddle masses in order to allow for the even-odd effect in the level densities.)

Note that the location of the Coulomb barrier is, in most cases under consideration here, irrelevant to the location of the maximum in the excitation function. The Coulomb barrier might begin to play a role for the very lightest reactions (^{48}Ca + ^{208}Pb is a case in point), where sticking occurs as a deeply sub-barrier process, and the resulting sticking cross section increases so rapidly with energy that it is able to delay the downturn of the fusion cross section by appreciably more than a fraction of an MeV.

Figure 11 compares the predicted theoretical excitation function for the reaction ^{58}Fe + ^{208}Pb → ^{265}108 + n with measurements. The effect of a 4 MeV energy dispersion due to the finite target thickness has been convoluted into the theoretical excitation function (dotted curve). Multiplication by 0.7 and a shift down by 0.5 MeV is necessary to bring the theory into agreement with the data. The width of the theoretical excitation function needs no adjustment. Figure 12 shows a similar comparison for the reaction ^{50}Ti + ^{208}Pb → ^{257}104 + n, and Fig. 13 for the reaction ^{54}Cr + ^{208}Pb → ^{261}106 + n. Figure 14 compares the less well-defined experimental excitation function for ^{64}Ni + ^{208}Pb → ^{271}110 + n with theory. Figure 15 compares with theory the two measured cross sections for the reaction ^{70}Zn + ^{208}Pb → ^{277}112 + n (one event at each of two energies). Figure 16 compares the excitation functions for the reaction ^{50}Ti + ^{209}Bi → ^{258}105 + n, and Fig. 17 for the reaction ^{64}Ni + ^{209}Bi → ^{272}111 + n. It will be seen that the absolute values of the cross sections

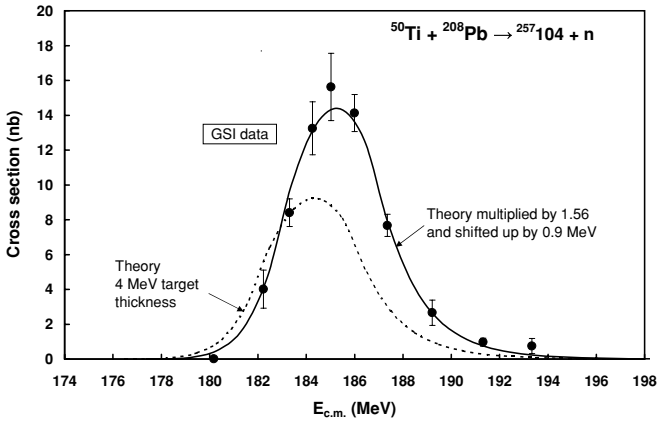

FIG. 12. This is like Fig. 11, but for the reaction ^{50}Ti + ^{208}Pb → ^{257}104 + n.

are typically off by up to a factor of 2 or so, and that the optimum bombarding energies are off by 1 or 2 MeV, as shown in Fig. 18.

B. The cross-bombardment scaling rule

An interesting insight is gained by comparing the calculated excitation functions for two 1n reactions leading to the same compound nucleus, such as the reactions ^{64}Ni + ^{209}Bi → ^{272}111 + n and ^{65}Cu + ^{208}Pb → ^{272}111 + n. Figure 19 shows these excitation functions plotted against the center of mass energy. Figure 20 shows them replotted against the energy excess over the effective thresholds for the respective reactions in order to exhibit the similarity of the excitation functions' intrinsic shapes. This is brought out vividly by the curve identified by the solid circles, obtained by multiplying the Cu + Pb excitation function by 1.90. The result is virtually indistinguishable from the Ni + Bi excitation function (open circles). This leads to the following scaling rule:

The excitation functions for two (neighboring) one-neutron-out heavy-ion reactions leading to the same compound nucleus by way of different target-projectile combinations,

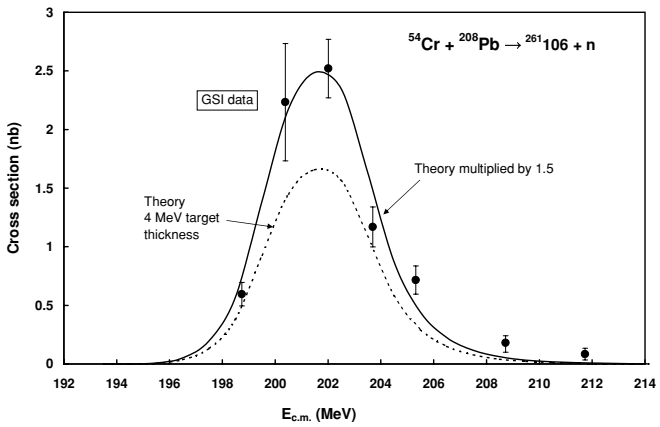

FIG. 13. This is like Fig. 11, but for the reaction ^{54}Cr + ^{208}Pb → ^{261}106 + n.

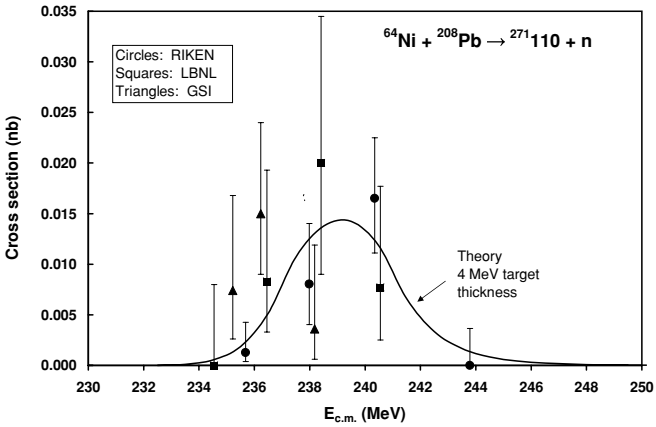

FIG. 14. This is like Fig. 11, but for the reaction ^{54}Ni + ^{208}Pb → ^{271}110 + *n*. The theoretical excitation function was neither scaled nor shifted.

when plotted against the energy excess above their respective effective reaction thresholds, to a good approximation differ only by a constant scaling factor.

We have used this rule to predict the excitation function for the ^{65}Cu + ^{208}Pb reaction from the measured ^{64}Ni + ^{209}Bi excitation function shown in Fig. 17, using the theoretical scaling factor 1.90. The result is shown in Fig. 21, together with a recent measurement. More decisive and comprehensive tests of this scaling rule for suitable pairs of reactions would be of considerable interest.

VI. HINDRANCE FACTORS IN HOT FUSION REACTIONS

So far, we have not applied our theory to *xn* reactions, but we have calculated the relevant hindrance factors, which bring out an important fact. Figure 22 shows these hindrance factors compared with the cold fusion hindrance factors. In both cases, the reactions refer to the synthesis of elements with the same atomic numbers $Z = 112$ to 118, but different neutron numbers, as shown in Fig. 1. In the case of hot fusion the hindrance factors were calculated for bombarding energies where the compound nucleus would be formed with excitations of 25, 35, and 45 MeV, at which around 2, 3, or 4 neutrons might be emitted. In all cases the same adjustable parameter was used, $s = 1.6$ fm. But it should be kept in mind that this value, deduced from a fit to reactions where a magic or near-magic target nucleus was used, may be different in the case of hot reactions, where the targets are not magic. In fact, it could well be that in the former reactions the loss of equilibrium against a neck growth was delayed because of the stiffness of the solid-like target nuclei. With the nonmagic targets, the loss of equilibrium might occur at somewhat larger separations, requiring a greater value of *s* to fit the data. The excitation energy dependence of the hindrance factors in Fig. 22 is relatively mild, and the striking feature is the reduction of the hindrances by 4 or 5 orders of magnitude in comparison with the case of cold fusion. It remains to be seen whether these favorable factors, when combined with the unfavorable reductions due to multiple neutron emission and a possible increase of the surface separation at which loss of equilibrium takes place,

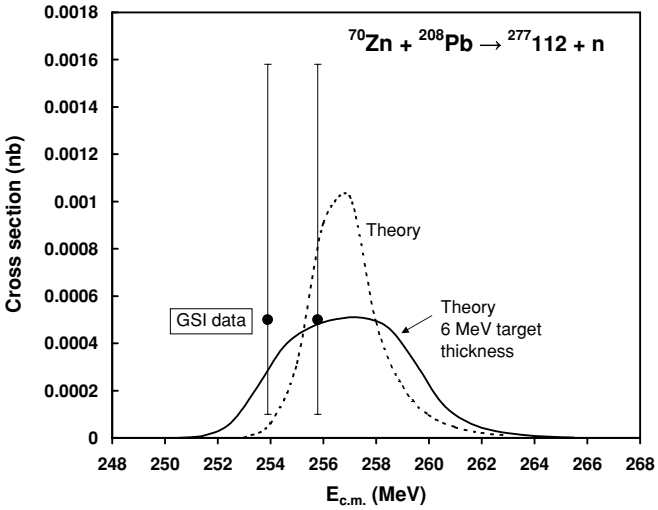

FIG. 15. This is like Fig. 11, but for the reaction ^{70}Zn + ^{208}Pb → ^{277}112 + *n*.

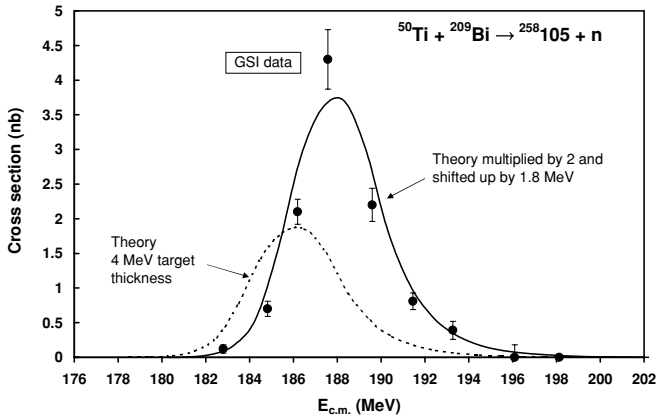

FIG. 16. This is like Fig. 11, but for the reaction ^{50}Ti + ^{209}Bi → ^{258}105 + *n*.

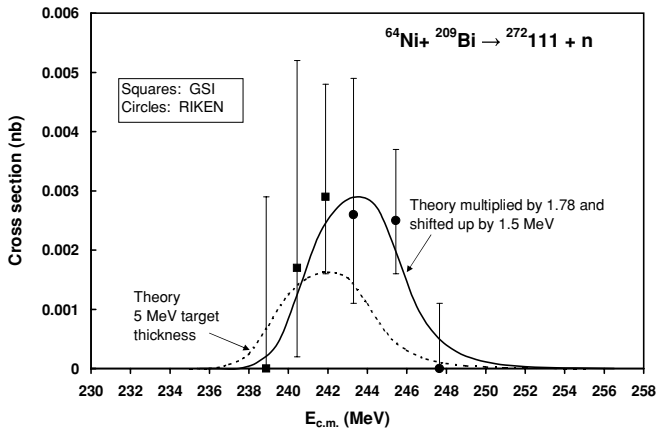

FIG. 17. This is like Fig. 11, but for the reaction ^{64}Ni + ^{209}Bi → ^{272}111 + *n*.

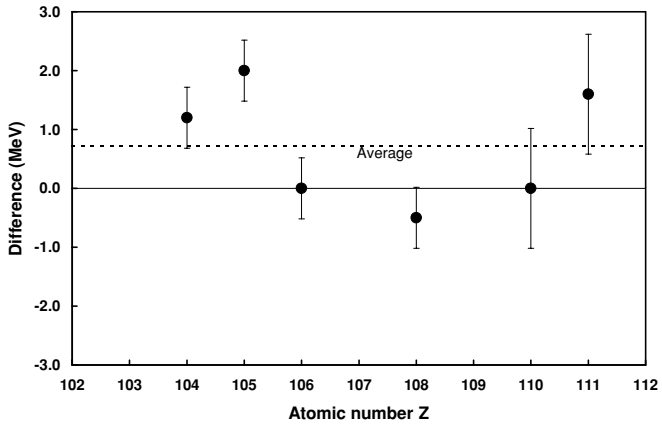

FIG. 18. The differences between measured and theoretical optimum center of mass energies deduced from Figs. 11 to 17.

are able to account for the cross sections measured in hot fusion reactions.

The two reasons for the reduction of the hindrance factors in Fig. 22 are the smaller barriers opposing diffusion and the higher temperatures, which together reduce considerably the critical factor H/T. The reduced barriers are plotted in Fig. 23. In the case of the relatively small projectile ^{48}Ca fusing with the very heavy targets from U to Cf, not only is the product Z_1Z_2 smaller but also, after neck growth, the system is more compact and closer to the maximum deformation energy where the barrier opposing diffusion would be zero.

VII. DISCUSSION

We made an attempt to interpret the cross sections for the synthesis of very heavy elements in one-neutron-out reactions, focusing in particular on reactions with ^{208}Pb and ^{209}Bi targets. We approximated the excitation functions by the product of the cross section to overcome the Coulomb barrier, times the probability that the resulting composite system overcomes by a diffusion process the barrier separating it from the compound-nucleus configuration, times the probability that the excited compound nucleus survives fission. Something like this general scheme is common to many current treatments of the subject (see, for example, [15,16]). Apart from technical details, the feature that distinguishes our approach is the concept of an injection of the system from the near-contact configuration into an "asymmetric fission valley." This represents an attempt to bypass the intricate dynamic process of the neck growth stage, which is especially difficult to treat in a realistic way. The hope here is to make use of the expected short time scale characterizing the neck growth. This shortness is due to the large driving force associated with the considerable saving of surface energy obtained by filling the crevice between the two juxtaposed nuclear surfaces, achieved at the cost of only a small adjustment of the nuclear density distribution. This means that, at least at first, the neck growth can be considered as proceeding with the overall elongation and asymmetry of the system approximately frozen. This leads the system toward the bottom of an asymmetric fission valley, defined by minimizing the potential energy—at fixed elongation and asymmetry—with respect to the neck degree of freedom. As the system approaches the bottom of this valley, we expect that the neck growth will slow down, the system will heat up owing to dissipative effects, and a stage of diffusive shape evolution will begin. (In the initial stages of neck growth, the system's temperature is close to zero, and one may be justified in disregarding thermal shape fluctuations.) This suggests an idealization in which the complicated dynamics

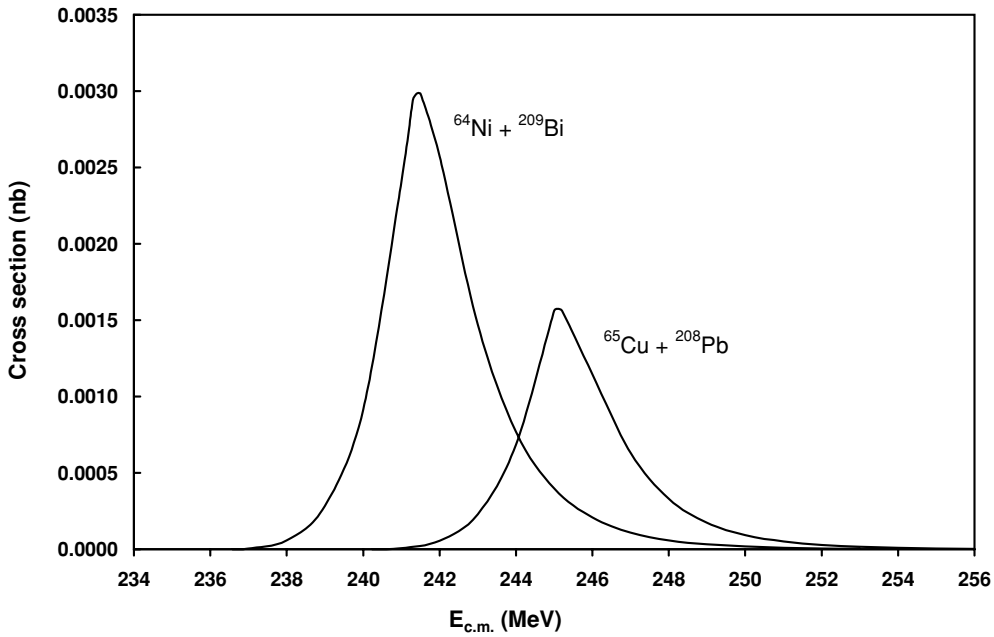

FIG. 19. The theoretical excitation functions for the reactions ^{64}Ni + ^{209}Bi and ^{65}Cu + ^{208}Pb leading to the same residual nucleus ^{272}111.

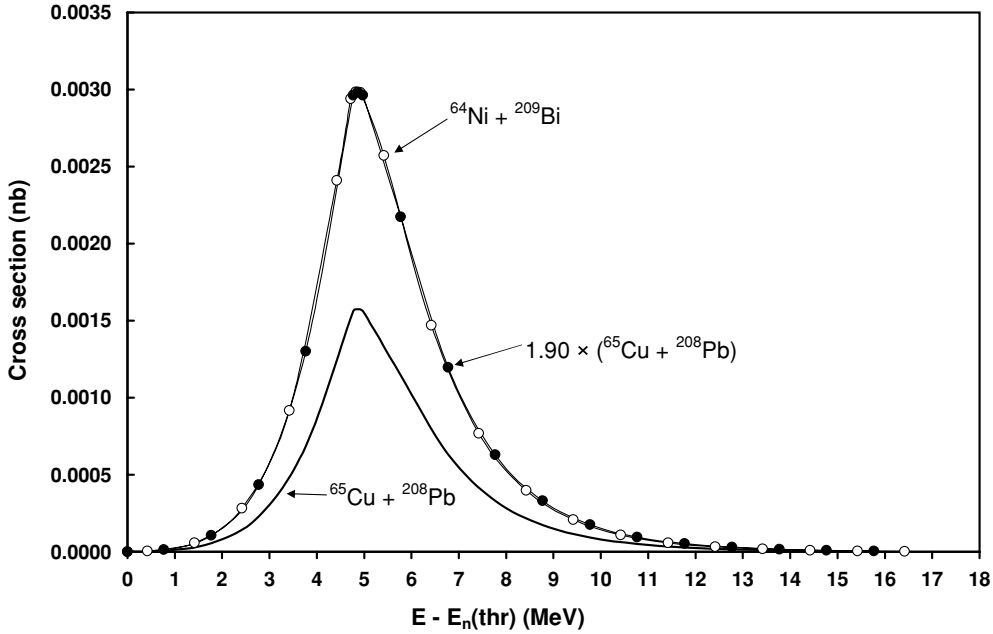

FIG. 20. The two excitation functions from Fig. 19 were replotted with respect to their effective reaction thresholds. The Cu + Pb excitation function was then scaled up by 1.90, which makes the result virtually indistinguishable from the Ni + Bi excitation function.

of neck growth and a gradual onset of diffusion is replaced by the sequence of two simpler processes: a schematic diffusion-free injection into the asymmetric fission valley, followed by a Brownian diffusion of probability beginning at some effective location in the valley, specified by the parameter s.

One may question the assumption that the subsequent diffusion continues to take place at fixed asymmetry, since with increasing neck radius the inhibition of the asymmetry degree of freedom disappears, and the system would find it profitable to evolve toward more symmetric shapes. This is because the lowest barrier guarding the compound nucleus configuration is associated with a symmetric saddle point. (The discussion so far is confined to the macroscopic part of the deformation energy. Shell effects will be mentioned presently.) Here we are fortuitously assisted by the nature of the parameterization of the nuclear shapes by two spheres connected by a hyperboloid for small necks, which goes over into a spheroid for large necks. With increasing neck size, the smoothly fitted spheroid begins to cover up an increasing fraction of the unequal spheres, whose size ratio formally defines the asymmetry. Hence the resulting shape, which eventually would actually become a (reflection symmetric) single spheroid, automatically tends to a symmetric configuration, even though it is formally a member of a family of shapes with frozen asymmetry. Thus, for very heavy systems, the energy of the macroscopic saddle in the asymmetric fission valley as calculated with our parameterization is expected to differ only slightly from the energy of the symmetric saddle point.

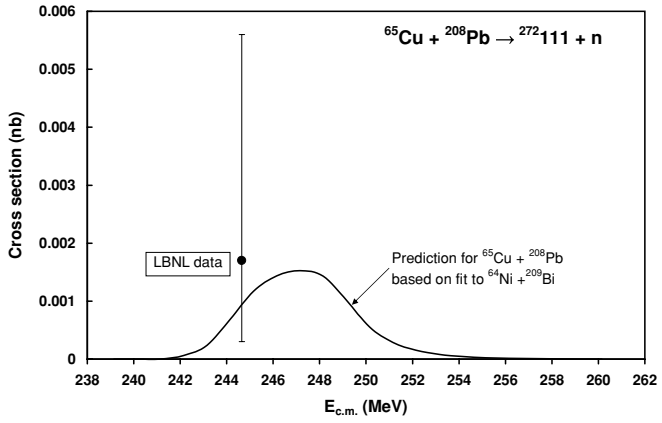

FIG. 21. The solid curve from Fig. 17, representing the measured excitation function for the ^{64}Ni + ^{209}Bi → ^{272}111 + n reaction, was used to predict the excitation function for the ^{65}Cu + ^{208}Pb → ^{272}111 + n reaction by dividing it by the theoretical scaling factor 1.90 and shifting it up by the difference in the effective reaction thresholds for the two reactions. A recent measurement (based on a single event) is shown.

All this having been said, it is clear that our injection scheme of bypassing the dynamics of neck growth is not a theory of the process, but rather a schematic prescription with a qualitative justification and the virtue of simplicity.

One may well question the disregard of shell effects in the deformation energy landscape along the asymmetric fission valley. (The shell effects in the initial fragments are, of course, taken into account, and so are shell effects in the compound nucleus and in the neutron-emission saddle-point mass. Shell effects in the fission saddle mass are expected to be small [17].) Some attenuation of shell effects in the asymmetric valley is to be expected because of the excitation of the system, and an indirect indication of the limited importance of shell structure in this stage of the process

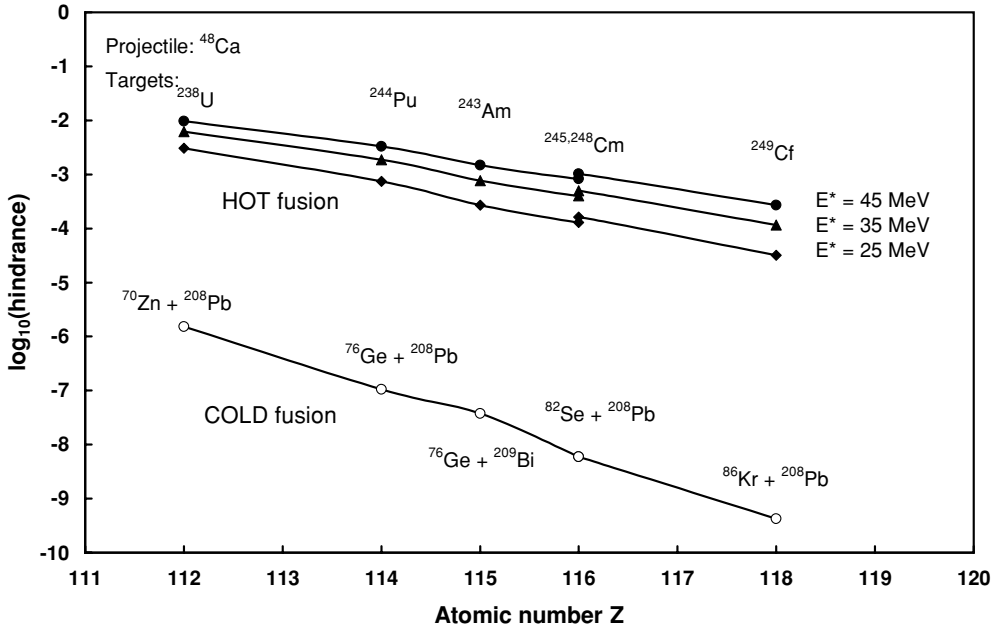

FIG. 22. The lowest curve shows the logarithms of the calculated hindrance factors in cold fusion reactions designed to make elements $Z = 112$–118. (See Fig. 2.) The excitation energies are typically 13–14 MeV. The upper curves show the hindrance factors when the same elements are made in hot fusion reactions at excitation energies of 25, 35, and 45 MeV. The hindrances are now less by 4 to 5 orders of magnitude.

comes from a comparison of our theory (without shell effects in the asymmetric fission valley) with the measured cross sections. In the set of 12 cross sections displayed in Fig. 2, there is at present no evidence for large discrepancies that could be attributed to the neglect of shell effects in the deformation energies. A realistic inclusion of such shell effects in the theory would, of course, complicate the calculations considerably.

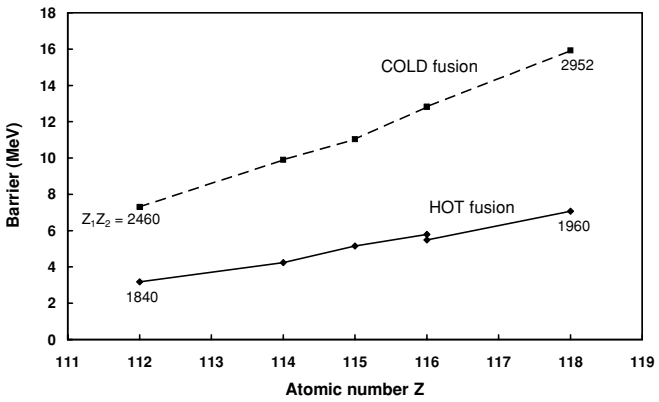

FIG. 23. The barriers opposing diffusion in cold fusion reactions to make elements 112 to 118 range from about 7 to 16 MeV (compare Fig. 8). In hot fusion reactions, the corresponding barriers range from 3 to 7 MeV. The reason is partly the reduced Coulomb repulsion, as indicated by the values of Z_1Z_2 listed along the curves. In addition, the injection configurations in the asymmetric fission valley are more compact and closer to the top of the barrier opposing diffusion, where the total repulsive force is zero.

With reference to Fig. 2 we may note the following. In the calculations there is one adjusted parameter, $s = 1.6$ fm, specifying the location in the asymmetric fission valley where diffusion is assumed to begin. As already mentioned, the calculated cross section for the reaction leading to $Z = 102$ is virtually independent of s (see Fig. 8) so the order of magnitude agreement with measurement in this case can be said to result without the help of an adjustable parameter. Changing s allows the overall decrease of the cross sections with increasing Z to be adjusted. The approximately linear trend of the logarithmic cross sections is reproduced, as are the major deviations from a smooth line. The illustrated extrapolation of the cross sections to the reactions with ^{76}Ge on ^{208}Pb and ^{209}Bi ($Z = 114$ and $Z = 115$) assumes that the corresponding compound nuclei are spherical. If, instead, we assumed that they continue to be deformed, the extrapolation would follow the trend of the cross sections for $Z = 111$, 112, and 113, resulting in predicted values about an order of magnitude smaller than shown in Fig. 2. As can be seen from Fig. 1, the landing places for $Z = 114$ and 115 are (according to calculations) on the boundary between the regions dominated by the deformed and spherical magic numbers. For $Z = 116$ to 119 the calculated compound nuclei are spherical. Taking the extrapolations at face value, the predicted cross section for the reaction $^{86}\mathrm{Kr} + {}^{208}\mathrm{Pb} \rightarrow {}^{293}118 + n$ is between 0.01 pb and 0.001 pb, about two orders of magnitude below the present upper limit [6]. One should not forget, however, that all these estimates hinge on the accuracy of the calculated shell effects in Fig. 1, which affect the neutron emission probabilities. These shell effects have been shown to agree well with measurements in the region of the deformed nuclei around $Z = 108$, $N = 162$, but the reliability of the extrapolation to the region of spherical nuclei is uncertain.

Somewhat different predictions for these very heavy nuclei are currently under discussion [18–21]. (The shell corrections we actually used were obtained by reading off the values from Fig. 1 in the first reference listed under [26] and applying a slight renormalization explained in App. B. More recent calculations from the second reference in [26] and private communication from Z. Patyk and A. Sobiczewski do not differ substantially from the older results. But a comprehensive study of the dependence of the predictions obtained using our theory on different theoretical estimates of the shell corrections remains to be carried out.)

A further serious concern regarding extrapolations from reactions involving deformed compound nuclei to reactions resulting in spherical nuclei is raised by the studies in [22], where the anticipated enhancement of cross sections associated with a spherical (residual) nucleus stabilized by a shell effect does not appear to be observed in the region $Z \approx 88, N \approx 126$.

As for other uncertainties and shortcomings of the present scheme, we should mention the limited accuracy of the extrapolated Coulomb barriers in Fig. 4 and, especially, the clearly quite uncertain extrapolation of the Gaussian widths in Fig. 6. (As noted before, this is critical for the lighter reactions, which rely on a sub-barrier process for sticking, but becomes less serious for the heaviest over-the-barrier reactions.) In the survival stage, there is also some uncertainty regarding the accuracy of the formula used for the ratio of the neutron to fission disintegration widths, based on [14]. The more conventional expression for this ratio has a pre-exponential factor that is typically greater by about a factor 3 than the one used here. This would aggravate the discrepancy with the lighter reactions in Fig. 2 (there is no recourse for them in the adjustable parameter s). The difference between the two formulas becomes serious for xn reactions, where the ratio of the two predictions would be proportional approximately to 3^n.

Finally, a remark on the overall objective of this study and the approach to the problem that we have adopted. In attempting to understand and interpret a set of experimental findings, two somewhat different approaches may be useful. In some cases, the physics is sufficiently unambiguous so that one is faced with simply finding the solution of a well-defined mathematical problem. (Examples include atomic problems, where the underlying Hamiltonian is to all intents and purposes well defined.) In other cases, and this includes many nuclear problems, especially of a dynamic character, the underlying Hamiltonian is not really defined. In those cases, a more creative approach is indicated: to invent a soluble model that has a chance of representing a significant part of the physics of the situation to be analyzed. In the case of the dynamic fusion of two nuclei, even idealized models, such as hydrodynamic or time-dependent Hartree-Fock schemes, are not easily soluble. In the present paper, we have gone one step further in simplifying the problem in that we have bypassed the dynamics of the neck growth phase by a conjectured injection into the asymmetric fission valley. The price we pay is the introduction of an adjustable parameter. The gain is that the whole procedure is now represented by algebraic equations rather than by computer outputs. There are two advantages here: operationally the scheme is very transparent, and the calculations are sufficiently simple, so that the model may be modified and experimented with using little effort. (To this end we have described in sufficient detail the formulas used, so that interested readers could do these explorations for themselves.) These advantages have to be weighed against the undoubted shortcoming that no well-defined model has actually been solved with controlled accuracy. Nevertheless, we believe that our study may be helpful in the interpretation of existing data and in extrapolations to novel situations.

ACKNOWLEDGMENTS

We thank S. Hofmann, K. Morita, and Yu. Ts. Oganessian for sharing their unpublished data with us, and Darleane Hoffman and C. M. Folden III for discussions, especially concerning recent experiments on the synthesis of elements 110 and 111. We thank Z. Patyk and A. Sobiczewski for providing us with unpublished results on properties of superheavy nuclei. This work was supported by the U.S. Department of Energy under Contract No. DE-AC0376SF00098 (LBNL) and by the Polish State Committee of Scientific Research (KBN).

APPENDIX A

For the sake of completeness we repeat here the content of App. B in Part I, supplemented with an improved treatment of the interpolation of the deformation energy in the asymmetric fission valley in the interval between the length of the system corresponding to contact and the length (diameter) of the compound nucleus.

The following formulas provide approximations to the macroscopic deformation energy, ΔE, in the asymmetric fission valley of a nucleus idealized as a uniformly charged drop. The shape of the drop, originally spherical with radius R, is parameterized by two spheres with radii R_1 and R_2 connected smoothly by a portion of a spheroid, cone, or hyperboloid [11,13]. Three variables specify a given shape: elongation, asymmetry, and neck size.

Let ξ denote the deformation energy in units of the surface energy E_s of the spherical shape. Let σ stand for the surface separation variable s in units of R (not to be confused with the cross section σ). Thus

$$\sigma = \frac{L - 2(R_1 + R_2)}{R}, \qquad \xi = \frac{\Delta E}{E_s}. \tag{A1}$$

For each value of s the macroscopic energy from [13] was minimized with respect to the neck variable at fixed asymmetry. In a range of parameters to be specified presently, the resulting deformation energy in its dependence on s was found to be reproduced to good approximation by the following quadratic:

$$\xi = a + b\sigma + c\sigma^2. \tag{A2}$$

The coefficients a, b, c are functions of the asymmetry Δ and of the fissility x defined as

$$\Delta = \frac{R_1 - R_2}{R_1 + R_2}, \tag{A3}$$

$$x = \frac{\text{Electrostatic energy of sphere}}{2E_s}. \tag{A4}$$

Using the notations $D = \Delta^2$ and $t = 1 - x$, we found

$$a = \alpha_a + \beta_a t + \gamma t^2, \tag{A5}$$

$$b = \alpha_b + \beta_b t, \tag{A6}$$

$$c = \alpha_c + \beta_c t, \tag{A7}$$

where

$$\alpha_a = -0.00557 - 0.01929\exp(-D/0.02283), \tag{A8}$$

$$\beta_a = 0.048 + 0.12151\exp(-D/0.04053), \tag{A9}$$

$$\gamma = -0.073 + 0.94D, \tag{A10}$$

$$\alpha_b = -0.01045 - 0.05303\exp(-D/0.03205), \tag{A11}$$

$$\beta_b = 0.019 + 0.25663\exp(-D/0.07331), \tag{A12}$$

$$\alpha_c = -0.02137 + 0.1944D, \tag{A13}$$

$$\beta_c = 0.0214 + 0.6158D. \tag{A14}$$

The above formulas have been tested for adequate accuracy in the range $0.85 < x < 1.05$, $-0.25 < \Delta < 0.25$, and $-0.1 < \sigma < 0.44$.

In the interval of lengths between contact, $L = 2(R_1 + R_2)$, and $L = 2R$ (the diameter of the compound nucleus) we shall use instead of Eq. (A2) the cubic

$$\xi = p(\sigma - \sigma_0)^2 - q(\sigma - \sigma_0)^3. \tag{A15}$$

Here σ_0 stands for the value of σ corresponding to the spherical compound nucleus

$$\sigma_0 = \frac{2R - 2(R_1 + R_2)}{R}. \tag{A16}$$

Using $R_1^3 + R_2^3 = R^3$, together with Eq. (A3), we find

$$\sigma_0 = 2 - \frac{4}{(2 + 6D)^{1/3}}, \tag{A17}$$

a negative quantity.

Demanding a smooth junction of Eqs. (A2) and (A15) at $\sigma = 0$, we readily find

$$p = \frac{b}{\sigma_0} + \frac{3a}{\sigma_0^2} \qquad \text{and} \qquad q = -\frac{b}{\sigma_0^2} - \frac{2a}{\sigma_0^3}. \tag{A18}$$

When the maximum in ξ is located for positive σ, Eq. (A2) is to be used, giving

$$\sigma_{\max} = -\frac{b}{2c} \qquad \text{and} \qquad \xi_{\max} = a - \frac{b^2}{4c}. \tag{A19}$$

When the maximum occurs for negative σ, Eq. (A15) gives

$$\sigma_{\max} = \sigma_0 + \frac{2p}{3q} \qquad \text{and} \qquad \xi_{\max} = \frac{4p^3}{27q^2}. \tag{A20}$$

The barriers opposing diffusion follow as $[\xi_{\max} - \xi(s)]E_s$. Note that Eq. (A20) is not to be used when p turns negative for very heavy systems. The maximum in ξ, equal to zero, is then located at the fixed value $\sigma_{\max} = \sigma_0$, i.e., at the (unstable) spherical compound-nucleus configuration. Note also that the use of a cubic when s is negative means that the barrier to be overcome by diffusion is no longer exactly parabolic, as assumed in the derivation of Eqs. (10) and (11). As can be verified with the aid of Fig. 8, the relevant parts of the deformation energies differ very little from parabolas, so the above equations should remain good approximations. The assumption of a constant temperature during the diffusion is not a serious defect for the lighter systems, when the barrier to be overcome is appreciably less than a typical excitation energy. It may become significant for the heaviest systems, when this is no longer the case. The use of the relatively high temperature based on the excitation at the injection point would tend to underestimate the hindrance for such reactions.

In the special case of symmetric configurations ($\Delta = 0$), Eq. (A15) reduces to

$$\xi = (0.5354\,t - 0.6347\,t^2)\alpha^2 - (0.1226 + 0.0750\,t - 0.7204\,t^2)\alpha^3, \tag{A21}$$

where α is the relative elongation $\alpha = (L - L_0)/L_0$. Equation (A21) may be used to calculate, for systems with fissility close to 1, the purely macroscopic saddle-point deformation energies, or to estimate corrections to the topographic theorem (see Sec. III). Note that the coefficients α_b and α_c in Eqs. (A11) and (A13) are slightly different than in [1]. This is the result of imposing the constraint that p should vanish when $D = 0$ and $t = 0$, which constraint was not enforced in [1].

The energy unit E_s and the fissility x were calculated using the parameters from [23], viz.

$$E_s = 17.9439(1 - 1.7826\,I^2)A^{2/3}\ \text{MeV}, \tag{A22}$$

$$x = \frac{Z^2/A}{50.883(1 - 1.7826\,I^2)}, \tag{A23}$$

where $I = (N - Z)/A$.

APPENDIX B

1. The level densities

The level density $\rho(U)$ for a nucleus of mass number A, in its dependence on shape and excitation energy U, is written as

$$\rho(U) = \exp[S(U)], \tag{B1}$$

where, for $U^* > 0$, the entropy $S(U)$ is given by [24,25]

$$S(U) = 2\sqrt{a\{U^* + \Delta_{\text{sh}}[1 - \exp(-U^*/k)]\}}, \tag{B2}$$

with $k = A^{1/3}/0.47$ and Δ_{sh} the shell correction, both in MeV, and

$$a = 0.076A + 0.180A^{2/3}F(\alpha) + 0.157A^{1/3}G(\alpha)\ \text{MeV}^{-1}. \tag{B3}$$

When $U^* < 0$ we set $\rho(U)$ equal to zero. Here

$$U^* = U - 24\ \text{MeV}/\sqrt{A} \qquad \text{for even-even nuclei,} \tag{B4}$$

$$= U - 12\ \text{MeV}/\sqrt{A} \qquad \text{for odd-}A\text{ nuclei,} \tag{B5}$$

$$= U \qquad \text{for odd-odd nuclei.} \tag{B6}$$

The last two terms in Eq. (B3) allow approximately for the shape dependence of the level density on the deformation variable α, defined by $(R_{\max} - R)/R$, where $R_{\max}$ is the semimajor axis of the (axially symmetric) nucleus of radius R before deformation (see Part I). The functions F and G are approximated by

$$F(\alpha) = 1 + (0.6416\alpha - 0.1421\alpha^2)^2 \tag{B7}$$

$$G(\alpha) = 1 + (0.6542\alpha - 0.0483\alpha^2)^2. \tag{B8}$$

These equations represent an attempt to take approximate account of deformation, pairing, and shell effects on the level densities [1]. Note that assuming the level density to be zero up to U^*, which differs from U by an even-odd correction, is equivalent to increasing the threshold for the reaction in question by this amount. This leads to the "effective" thresholds used in Sec. IV.

The shell corrections $\Delta_{\rm sh}$ for the ground states were read off of Fig. 1 (taken from [26]) and modified slightly as follows. Since for the macroscopic part of the nuclear mass of a spherical nucleus we use the Thomas-Fermi value $M_{\rm TF}$ [27], the sum $M_{\rm TF} + \Delta_{\rm sh}$ represents the predicted mass of a nucleus. We found that using the shell effect from [26], this mass is, on average, lower than the measured mass by 0.69 MeV for even-even nuclei, by 0.31 MeV for even-Z, odd-N nuclei, by 0.43 MeV for odd-Z, even-N nuclei, and by 0.2 MeV for odd-odd nuclei. (For each nuclear type, there were four cases in the region of interest where the predictions could be compared with measurements.) Thus the corrected shell effects that we adopted are a little less negative than those in [26].

To evaluate (approximately) the integrals in Eq. (12), we expand the entropies about the upper limits of integration and obtain

$$\frac{\Gamma_n}{\Gamma_f} = \frac{T_n[1 - \exp(-U_n/T_n)]\exp S_n}{T_f[1 - \exp(-U_f/T_f)]\exp S_f}, \tag{B9}$$

where the temperatures T_n, T_f stand for the reciprocals of the entropy derivatives S_n' and S_f' which, together with S_n and S_f, are all evaluated at the appropriate upper limits.

2. The saddle-point masses

For the saddle-point masses, we used a slightly modified topographic theorem, which states that a fission saddle-point mass is approximately equal to the macroscopic saddle mass with shell effects disregarded [17]. The modification concerns cases when the fissility parameter is close to 1, and the macroscopic saddle-point shape is close to the sphere. The macroscopic saddle-point mass is then close to that of the spherical shape; however, if the nucleus is stabilized by a shell effect (especially if the ground state is deformed), the saddle-point shape may be quite significantly elongated, and the macroscopic mass at that elongation will be somewhat less than the mass of the sphere. Thus, even if the shell correction itself at that location is disregarded in the spirit of the topographic theorem, the saddle-point deformation energy, as approximated by the macroscopic part, will be somewhat negative. To apply this correction to the topographic theorem, one needs to know the deformation of the saddle-point shape in question and the macroscopic energy at that deformation. In the results presented in the present paper, the former were provided to us by R. Smolanczuk (private communication), and the latter were calculated using the Thomas-Fermi model [27]. Since such Thomas-Fermi calculations of deformation energies are not generally available, an alternative is to use the macroscopic deformation energies described in App. A, this time for symmetric configurations with $\Delta = 0$ [Eq. (A.21)]. A comparison of the saddle-point deformation energies obtained in this way with the Thomas-Fermi results shows that the former is greater by 0.67 MeV for the lightest compound nucleus considered here (^{256}No), but the difference becomes almost negligible for the heaviest, especially in cases where the shell-stabilized nucleus is spherical.

In cases where the saddle deformation is not known, the following rule of thumb may be useful: If the ground state of the heavy compound nucleus with fissility x close to 1 is stabilized by a spherical shell effect, the major semiaxis of the saddle configuration will exceed the radius of the spherical configuration by about 1.5 fm. If the ground state is well deformed due to a shell effect, the corresponding difference will be about 2.5 fm. This is probably a rather rough rule, but in the present context it is used only to estimate the relatively small correction to the topographic theorem. The (corrected) topographic theorem itself is to be used only in the sense of a reference baseline for the saddle-point masses; deviations of about an MeV, caused by shell effects at the saddle, are to be expected.

[1] W. J. Świątecki, K. Siwek-Wilczyńska, and J. Wilczyński, Acta Phys. Pol. **34**, 2049 (2003).

[2] W. J. Świątecki, K. Siwek-Wilczyńska, and J. Wilczyński, Intl. J. Mod. Phys. E **13**, 261 (2004).

[3] S. Hofmann, Rep. Prog. Phys. **61**, 639 (1998) and private communication.

[4] K. Morita, private communication; K. Morita, *et al*., J. Phys. Soc. Japan **73**, 1738 (2004).

[5] C. M. Folden III, K. E. Gregorich, Ch. E. Duellmann, H. Mahmood, G. K. Pang, J. M. Schwantes, R. Sudowe, P. M. Zielinski, H. Nitsche, and D. C. Hoffman, Phys. Rev. Lett. (to be published).

[6] K. E. Gregorich, *et al*., Eur. Phys. J. **A18**, 633 (2003).

[7] N. Rowley, G. R. Satchler, and P. H. Stelson, Phys. Lett. **B245**, 25 (1991).

[8] K. Siwek-Wilczyńska and J. Wilczyński, Phys. Rev. C **69**, 024611 (2004).

[9] W. D. Myers and W. J. Świątecki, Phys. Rev. C **62**, 044610 (2000).

[10] P. Möller, J. R. Nix, W. D. Myers, and W. J. Swiatecki, At. Data Nucl. Data Tables **59**, 185 (1995).

[11] J. P. Blocki, H. Feldmeier, and W. J. Swiatecki, Nucl. Phys. **A459**, 145 (1986).

[12] H. Riske, *The Fokker-Planck Equation* (Springer-Verlag, Berlin, 1989).
[13] J. Blocki and W. J. Swiatecki, Lawrence Berkeley Laboratory preprint LBL-12811, May 1982 (unpublished).
[14] W. J. Swiatecki, Aust. J. Phys. **36**, 641 (1983).
[15] C. Shen, G. Kosenko, and Y. Abe, Phys. Rev. C **66**, 061602 (2002); Y. Abe and B. Bouriquet, Acta Phys. Pol. **B34**, 1927 (2002); Y. Abe, D. Boilley, G. Kosenko, and C. Shen, Acta Phys. Pol. **B34**, 2091 (2003).
[16] V. I. Zagrebaev, Phys. Rev. C **64**, 034606 (2001); Phys. Rev. C **65**, 014607 (2002); M. G. Itkis, Yu. Ts. Oganessian, and V. I. Zagrebaev, Phys. Rev. C **65**, 044602 (2002).
[17] W. D. Myers and W. J. Świątecki, Phys. Rev. C **60**, 014606 (1999).
[18] S. Ćwiok, J. Dobaczewski, P.-H. Heenen, P. Magierski, and W. Nazarewicz, Nucl. Phys. **A611**, 211 (1996).
[19] M. Bender, K. Rutz, P.-G. Reinhard, J. A. Maruhn, and W. Greiner, Phys. Rev. C **60**, 034304 (1999).
[20] K. Rutz, M. Bender, T. Burvenich, P.-G. Reinhard, J. A. Maruhn, and W. Greiner, Phys. Rev. C **56**, 238 (1997).
[21] A. T. Kruppa, M. Bender, W. Nazarewicz, P.-G. Reinhard, T. Vertse, and S. Ćwiok, Phys. Rev. C **61**, 034313 (2000).
[22] A. Heinz, *et al*., Nucl. Phys. **A713**, 3 (2003).
[23] W. D. Myers and W. J. Swiatecki, Ark. Fys. **36**, 343 (1967).
[24] A. V. Ignatyuk, G. N. Smirenkin, and A. S. Tishin, Sov. J. Nucl. Phys. **21**, 255 (1975).
[25] S. F. Mughabghab and C. Dunford, Phys. Rev. Lett. **81**, 4083 (1998).
[26] R. Smolańczuk, J. Skalski, and A. Sobiczewski, in *Proc. Int. Hirschegg Workshop XXIV, Extremes of Nuclear Structure*, edited by H. Feldmeier, J. Knoll, and W. Hornberg (GSI, Darmstadt, Germany, 1996), p. 4. See also I. Muntian, S. Hofmann, Z. Patyk, and A. Sobiczewski, Acta Phys. Pol. **B34**, 2073 (2003).
[27] W. D. Myers and W. J. Swiatecki, Nucl. Phys. **A601**, 141 (1996); Lawrence Berkeley Laboratory preprint LBL-36803, December 1994 (unpublished), available on http://ie.lbl.gov/txt/ms.txt.